# UCSF
## UC San Francisco Previously Published Works

**Title**

Intravital imaging reveals distinct responses of depleting dynamic tumor-associated macrophage and dendritic cell subpopulations

**Permalink**

https://escholarship.org/uc/item/8sw7g383

**Journal**

Proceedings of the National Academy of Sciences of the United States of America, 111(47)

**ISSN**

0027-8424

**Authors**

Lohela, Marja
Casbon, Amy-Jo
Olow, Aleksandra
et al.

**Publication Date**

2014-11-25

**DOI**

10.1073/pnas.1419899111

Peer reviewed

# Intravital imaging reveals distinct responses of depleting dynamic tumor-associated macrophage and dendritic cell subpopulations

Marja Lohela[a,1], Amy-Jo Casbon[a], Aleksandra Olow[a,2], Lynn Bonham[b,3], Daniel Branstetter[b], Ning Weng[b], Jeffrey Smith[b], and Zena Werb[a,4]

[a]Department of Anatomy, University of California, San Francisco, CA 94143; and [b]Amgen Corporation, Seattle, WA 98119

Tumor-infiltrating inflammatory cells comprise a major part of the stromal microenvironment and support cancer progression by multiple mechanisms. High numbers of tumor myeloid cells correlate with poor prognosis in breast cancer and are coupled with the angiogenic switch and malignant progression. However, the specific roles and regulation of heterogeneous tumor myeloid populations are incompletely understood. CSF-1 is a major myeloid cell mitogen, and signaling through its receptor CSF-1R is also linked to poor outcomes. To characterize myeloid cell function in tumors, we combined confocal intravital microscopy with depletion of CSF-1R–dependent cells using a neutralizing CSF-1R antibody in the mouse mammary tumor virus long-terminal region-driven polyoma middle T antigen breast cancer model. The depleted cells shared markers of tumor-associated macrophages and dendritic cells (M-DCs), matching the phenotype of tumor dendritic cells that take up antigens and interact with T cells. We defined functional subgroups within the M-DC population by imaging endocytic and matrix metalloproteinase activity. Anti–CSF-1R treatment altered stromal dynamics and impaired both survival of M-DCs and accumulation of new M-DCs, but did not deplete Gr-1+ neutrophils or block doxorubicin-induced myeloid cell recruitment, and had a minimal effect on lung myeloid cells. Nevertheless, prolonged treatment led to delayed tumor growth, reduced vascularity, and decreased lung metastasis. Because the myeloid infiltrate in metastatic lungs differed significantly from that in mammary tumors, the reduction in metastasis may result from the impact on primary tumors. The combination of functional analysis by intravital imaging with cellular characterization has refined our understanding of the effects of experimental targeted therapies on the tumor microenvironment.

inflammation | myeloid cells | matrix metalloproteinase | CSF-1 receptor | lung metastasis

Cells of the myeloid lineage, including macrophages, monocytes, neutrophils, mast cells, and immature myeloid cells, are major components of the complex stromal microenvironment of solid tumors (1, 2). Abundant evidence from human and experimental tumor types shows that myeloid cells support tumor growth and progression by a wide range of mechanisms, including stimulation of angiogenesis, secretion of factors inducing tumor growth, survival and cell migration, remodeling of the extracellular matrix to facilitate growth and invasion, recruitment of additional support cells, and suppression of the antitumor immune response (3–5). In human breast cancer, as in most other solid tumors, large numbers of myeloid cells, characterized as tumor-associated macrophages (TAMs), correlate with poor prognosis, as does high expression of the myeloid cell mitogen colony-stimulating factor-1 (CSF-1, M-CSF) or its receptor CSF-1R (CD115, c-fms), and gene-expression profiles reflecting myeloid involvement or CSF-1 signaling (3, 5–8).

The marked effects of myeloid cells on tumor growth, invasion, and metastasis identify them and the signaling pathways mediating cancer cell–myeloid cell interactions as potentially attractive targets for treatment of aggressive cancer. TAM depletion by clodronate-encapsulated liposomes reduces tumor growth in various grafted tumors (3, 5, 9). Genetic ablation, antisense and antibody approaches for inhibition of CSF-1/CSF-1R signaling lead to macrophage depletion and reduce malignancy in several models, with abrogated tumor angiogenesis in most cases (3, 5, 9, 10, and references therein). A null mutation in CSF-1, which leads to the lifelong absence of the majority of macrophages, results in delayed tumor progression in the transgenic mouse mammary tumor virus long terminal region-driven polyoma middle T antigen (MMTV-PyMT) model of aggressive breast cancer, evidenced by more differentiated histology and decreased lung metastasis, apparently because of decreased tumor angiogenesis (11–13).

Our understanding of the properties and functions of myeloid cell types in primary and metastatic tumors is still incomplete, because of the broad specificity and varying use of cellular markers, as well as myeloid cell plasticity and contrasting results obtained from a wide variety of tumor models (4, 14–16). We and others have used intravital microscopy to define real-time dynamics of several distinct subpopulations of stromal cells in different stages of mammary tumor progression and tumor response to chemotherapy, or relapse thereafter (17–20). In this study, we sought to define

---

## Significance

Tumor-infiltrating myeloid cells fail to support antitumor immunity, and instead contribute to increased malignancy and poor prognosis in breast cancer. We used intravital microscopy in a model of breast cancer to provide unique insight into cellular composition and real-time dynamics of the stromal microenvironment. We characterized the effects of targeted therapy against CSF-1R, an important myeloid cell mitogen receptor. We demonstrate that by blocking accumulation and compromising survival, anti–CSF-1R treatment depletes a cell population sharing characteristics of tumor-associated macrophages and dendritic cells, which further comprises subgroups with different endocytic and matrix metalloproteinase activities. However, the resulting relatively modest delay in tumor growth and metastasis suggests that other cells, such as neutrophils or fibroblasts, may maintain the tumor trophic microenvironment.

the characteristics and importance of CSF-1–dependent myeloid cells in the MMTV-PyMT breast cancer model by using the neutralizing monoclonal CSF-1R antibody M279 (21) to deplete this population at different stages of tumor progression. We then analyzed the tumor response, phenotype of the depleted cells, and cell dynamics in the tumor microenvironment.

## Results

**CSF-1R Blockage Depletes TAM-Dendritic Cells, but Does Not Affect Tumor-Associated Neutrophils.** We first established the efficacy of live imaging and flow cytometry for characterizing the regulation of CSF-1R–bearing myeloid cells in the MMTV-PyMT tumors (17). Treatment of tumor-bearing MMTV-PyMT/c-fms-EGFP

mice with M279 for 60 d dramatically reduced the numbers of c-fms-EGFP–expressing myeloid cells by ∼85% compared with rat IgG-treated control mice (Fig. 1A). M279 treatment also led to a massive increase of CSF-1 levels in the serum (Fig. S1A) because of the diminished clearance of the circulating ligand through CSF-1R–mediated endocytosis (21, 22). Immunostaining of tumor sections confirmed that cells expressing CSF-1R and the mature macrophage/TAM marker F4/80 were depleted throughout the tumor tissue (Fig. S1 C and D). Depletion of myeloid cells was also visible by intravital imaging of fourth (inguinal) mammary tumors of MMTV-PyMT/ACTB-ECFP/c-fms-EGFP mice with a spinning-disk confocal microscope (17, 18) as early as 1 wk of treatment in various tumor stages (Fig. 1B and Movies S1–S4). Depletion
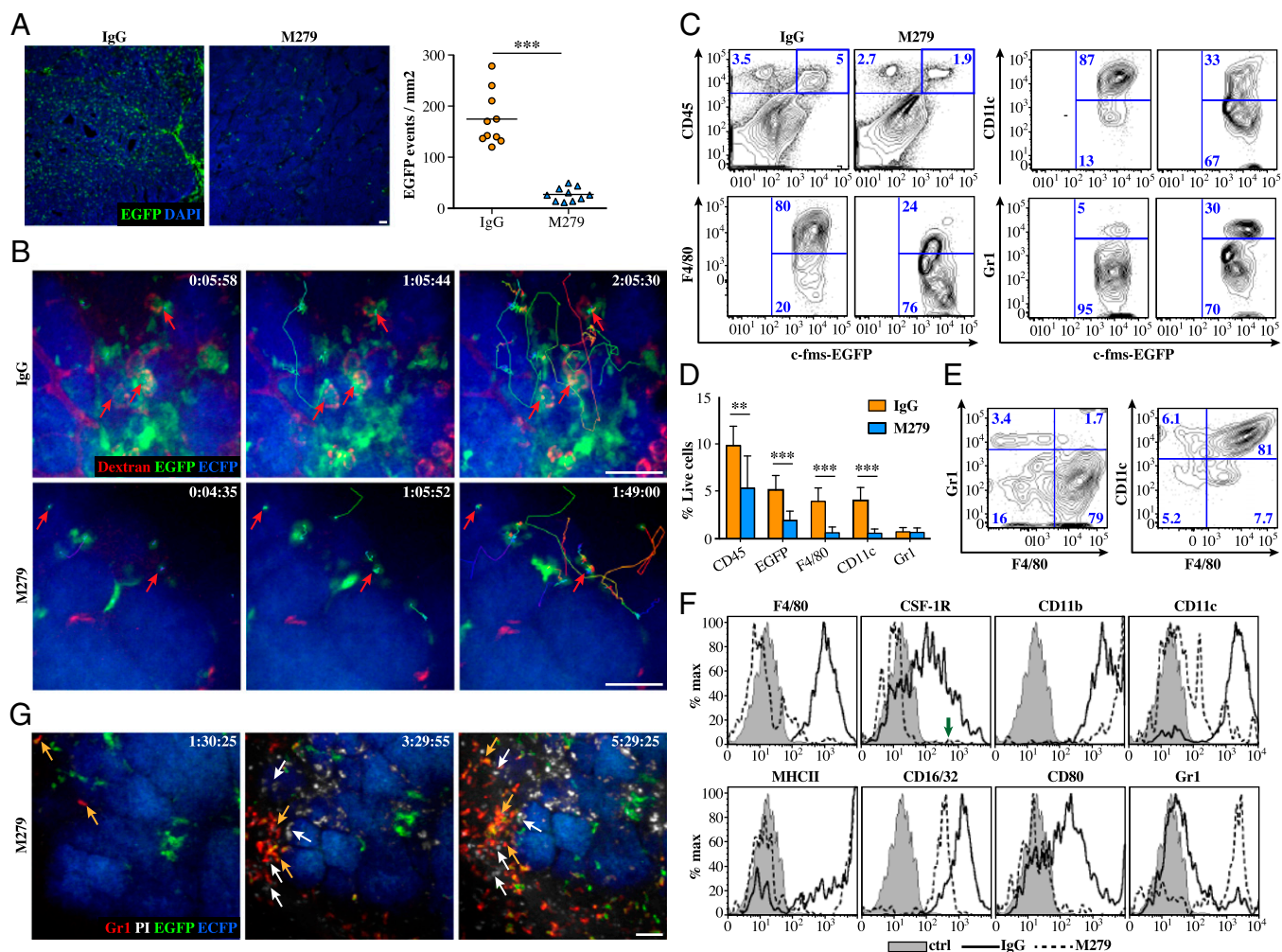


**Fig. 1.** Anti–CSF-1R efficiently depletes F4/80+ CD11c+ M-DCs, but does not affect Gr-1+ neutrophils/suppressor cells in tumors. (A) Representative micrographs of cryosections and quantification of myeloid cells from MMTV-PyMT/c-fms-EGFP mice treated from 8.5 wk (palpable stage) to 17-wk-old with M279 or IgG. (Scale bar, 50 μm.) n = 10 mice per group, ***P < 0.001. (B) Still frames from intravital imaging of MMTV-PyMT/c-fms-EGFP/ACTB-ECFP mice treated with M279 or IgG for 7 d, starting at 8 wk of age. Rhodamine-labeled 70 kDa dextran was injected intravenously 3–4 h before the start of imaging. Red arrows point to sessile dextran-positive cells, and tracks show the paths taken by individual cells. (Scale bar, 50 μm.) (C–E) Flow cytometric analysis of single cells isolated from tumors in MMTV-PyMT/c-fms-EGFP mice treated for 2–7 wk with M279 or IgG. (C) Characterization of CD45+ EGFP+ tumor myeloid cell populations using cell surface markers F4/80, CD11c, and Gr-1. (D) Quantification of the cell populations in C, using the gating strategies illustrated. Graph depicts means ± SD as percentages of total single cells in tumor, n = 7 mice (IgG) or 11 mice (M279) per group, ***P < 0.001. (E) Evaluation of CD45+ EGFP+ myeloid cells coexpressing F4/80 and CD11c or F4/80 and Gr-1. The majority of the EGFP+ cells are F4/80+ CD11c+, with minor single-positive populations. A small Gr-1+ population is also present. (F) Representative histograms characterizing the phenotype of CD45+ EGFP+ cells in IgG- and M279-treated tumors. Note the efficient depletion of cells expressing CSF-1R on the surface in M279-treated tumors (green arrow). See Fig. S2 for histograms of cell numbers. (G) Still frames from intravital imaging of a MMTV-PyMT/c-fms-EGFP/ACTB-ECFP mouse pretreated with M279 for 3 wk, starting at 9 wk of age, and the treated with a combination of M279 and doxorubicin chemotherapy for an additional 3 wk. The last doxorubicin dose was given 25 h before imaging. AF647-labeled Gr-1 antibody (pseudocolored red) was injected intravenously 1 h before imaging. Propidium iodide (pseudocolored white) was administered intraperitoneally every hour during imaging. Gr-1+ EGFP+ neutrophils (orange arrows) are recruited as doxorubicin-induced cell death (white arrows) increases. (Scale bar, 50 μm.)

visually estimated as more than 50% in M279- versus IgG-treated mice was seen in 6 of 11 of littermate pairs treated for 4–7 d, in 8 of 9 pairs treated for 14–25 d, and in 6 of 7 pairs treated for 30 d or longer. All M279- and control-treated tumors imaged had motile as well as stationary c-fms-EGFP$^+$ cells. M279 treatment resulted in a striking reduction in sessile stromal myeloid cells that take up intravenously injected low molecular weight dextran leaking out of the blood vessels (Fig. 1B, Fig. S1B, and Movies S1–S4). For a more rigorous quantification and characterization of the depletion effect, including the tumors and deeper tumor regions not accessible by intravital imaging, we used immunostaining of tumor sections and flow cytometry.

Flow cytometric analysis confirmed that M279 treatment efficiently depleted cells with surface expression of CSF-1R (Fig. 1F, green arrow). We next characterized the CSF-1R$^+$ cells. CSF-1R may be present on dendritic cells as well as macrophages (23). Strikingly, the depleted cells expressed the classical dendritic cell markers CD11c and MHC II, as well as F4/80, CD80, and CD11b (Fig. 1 C–F and Fig. S2A). Thus, these cells match the phenotype of the cells recently defined as tumor dendritic cells (TuDCs) in the MMTV-PyMT model (20), but have been called TAMs on the basis of CSF-1R and F4/80 expression in previous studies (24), and more recently, based on expression profiling (2). In our study, we refer to them as macrophage-dendritic cells (M-DCs). Indeed, the population expressing both F4/80 and CD11c constituted ∼80% of c-fms-EGFP–expressing myeloid cells in MMTV-PyMT tumors, with minor single-positive populations (Fig. 1E).

Motile Gr-1$^+$ cells patrol the tumor vessels and stroma (17). The Gr-1 antibody recognizes a heterogeneous population of myeloid cells, including neutrophils and inflammatory monocytes (25). Although neutrophils express the c-fms-EGFP transgene, they do not normally express the CSF-1R protein on the cell surface (26). Thus, the morphology of Gr1$^+$, FACS sorted cells was assessed to define the tumor-infiltrating Gr-1$^+$ populations. Approximately 90% of the cells had multiple nuclear lobes (Fig. S2B), characteristic of neutrophils. Whereas the frequency of Gr-1 cells was not changed by the M279 treatment (21), their relative proportion within c-fms-EGFP$^+$ myeloid cells increased markedly with the depletion of the large M-DC population (Fig. 1 C, D, and F, and Fig. S2A). Indeed, many of the motile c-fms-EGFP$^+$ cells in M279-treated tumors labeled with an injected Gr-1 antibody (Fig. 1G and Movie S5). Gr-1$^+$ cells are rapidly recruited in large numbers in response to cell death or necrotic debris (17, 18). However, M279 treatment did not disrupt the influx of Gr-1 cells to areas of cell death induced by the chemotherapy agent doxorubicin administered 24 h before imaging (Fig. 1G and Movie S6) (influx of cells was seen in four of six imaged mice in the IgG group and five and five mice in the M279 group when movies of two to six locations in each tumor were analyzed). These results suggest that CSF-1R–independent myeloid cells can contribute significantly to the tumor microenvironment.

**M-DCs Depleted by Anti–CSF-1R Treatment Include a Sessile, Endocytic Subgroup with Matrix Metalloproteinase Activity.** The macrophage mannose receptor (MMR/CD206), a marker of alternative activation/M2 type polarization (17, 27), mediates dextran uptake by myeloid cells. Dextran uptake has been used to identify TAMs (17, 24) and is suggested as a surrogate marker for antigen uptake by TuDCs (20). The dextran-ingesting cells, located around the tumor nodules in the MMTV-PyMT model, were markedly decreased in M279-treated tumors (Figs. 1B and 2 C and F). As expected, very few Gr-1–expressing cells showed dextran uptake (Fig. 2 A and E). The dextran-positive cells were a subpopulation of M-DCs, representing approximately one-third of them; >90% of dextran-positive cells expressed high levels of F4/80, and all were positive for CD11c (Fig. 2 A and E). Most of the depleted dextran-ingesting cells also expressed lymphatic vessel endothelial hyaluronan re-

ceptor-1 (LYVE-1) (Fig. 2G and Fig. S1E), a marker of M2-type and fetal macrophages with potent angiogenic activity and a tissue remodeling phenotype (28–32). The dextran-positive cells were depleted as efficiently as the total F4/80 population (Fig. 2 B–D).

Matrix metalloproteinases (MMPs), and the activity of MMP9 in particular, are important for tumor trophic functions of TAMs and Gr-1$^+$ neutrophils/inflammatory monocytes (18, 33–37). When we imaged tumors with MMPSense, a fluorescent probe for the proteolytic activity of MMPs 2, 7, 9 and 13, most c-fms-EGFP$^+$, dextran-ingesting myeloid cells displayed MMP activity (Fig. 2 H and I, and Movies S7 and S8). MMPSense-labeled cells were also dramatically depleted by M279 treatment (Fig. 2I and Movies S8 and S9). The rapidly moving Gr-1$^+$ cells did not label with MMPSense (Fig. 2I and Movies S8 and S9), suggesting that their MMP9 was in an inactive state or diluted beyond detection upon secretion. These data suggest that the c-fms-EGFP$^+$, MMPSense-labeled cells may play a role in promoting tissue remodeling involved in angiogenesis, invasion, and metastasis.

**Anti–CSF-1R Acts by Blocking the Accumulation of New Myeloid Cells and Compromising the Survival of Existing Tumor M-DCs.** CSF-1/CSF-1R signaling can support myeloid cell migration and differentiation, as well as their proliferation and survival (38). Systemic anti–CSF-1R treatment in tumor-bearing mice could block the arrival of new M-DCs into tumors by directly removing the chemotactic signal and the stimulus for local differentiation or proliferation, or deprive existing M-DCs of an essential survival signal, causing them to die. To test these possible mechanisms, we injected MMTV-PyMT mice bearing small tumors with rhodamine-labeled dextran at the start of a 2-wk M279 or IgG treatment, and then injected Alexa Fluor (AF)647-labeled dextran 1–2 h before collecting tumors for analysis. We observed that the dextran-ingesting cells were long-lived, because in control mice, a large number of rhodamine-dextran–positive myeloid cells were still present after the 2-wk chase. These rhodamine-labeled cells took up the AF647-dextran 2 wk later. However, we also saw a robust infiltration of myeloid cells that were positive for AF647-dextran only, which we interpret as the cell population either recruited from peripheral blood or born by local proliferation or differentiation during the 2-wk chase (Fig. 3A). Interestingly, we observed a sharp drop in the numbers of both dextran double-positive (preexisting) and AF647-dextran single-positive (new) myeloid cells in the M279-treated tumors (Fig. 3 A and B). These data suggest that M279 treatment blocks the survival of preexisting M-DCs in the tumor, and also inhibits further accumulation of new M-DCs. To exclude the possibility that dextran ingestion sensitizes M-DCs to M279 treatment, compromising survival, we used propidium iodide labeling in conjunction with intravital imaging to detect tumor myeloid cell death in vivo. In mice not injected with dextran, we saw multiple c-fms-EGFP$^+$ cells in the tumor labeling with propidium iodide after 4–6 d of M279 treatment, compared with very rare propidium iodide-positive myeloid cells in control tumors, confirming that CSF-1R inhibition can result in myeloid cell death (Fig. 3C and Movies S10 and S11) (myeloid cell death was seen in three of seven mice in the M279 group and none of the five mice in the IgG group when two to eight locations in each tumor were analyzed).

Because the accumulation of new M-DCs into tumors was impaired, we characterized the myeloid cell populations in peripheral blood by flow cytometric analysis. There was no difference in the total myeloid cell pool in the blood of M279-treated versus control mice, and the Gr-1$^+$ population, which greatly expands in blood during tumor progression, was unchanged by M279 treatment (Fig. 3 D, F, and H). However, expression of CSF-1R was lower in blood cells (Fig. S3A). Intravenous injection of AF647-labeled M279 revealed a small CSF-1R$^+$ population expressing very high levels of F4/80 (Fig. S3B). In
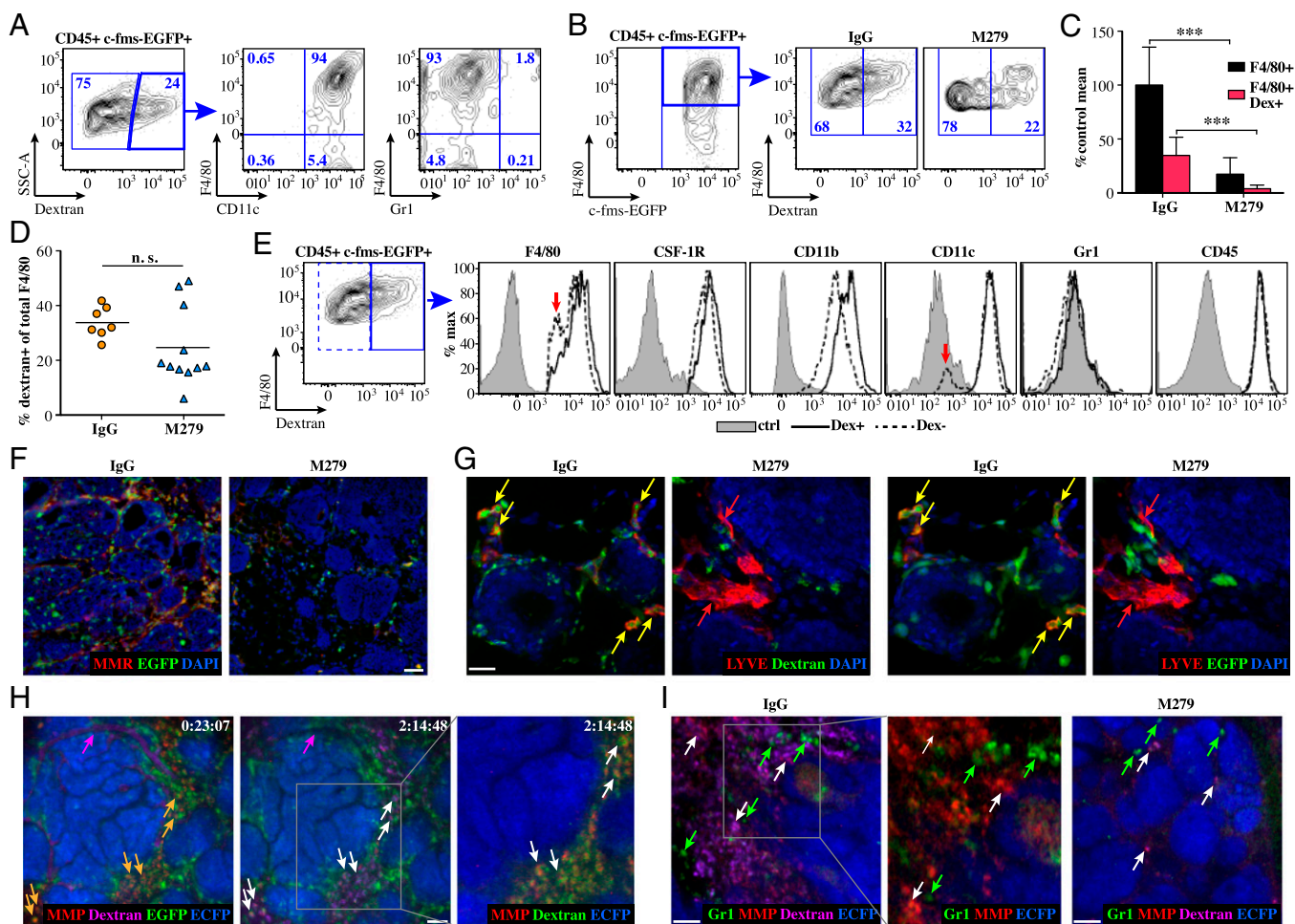
**Fig. 2.** M-DCs depleted by anti–CSF-1R treatment contain subpopulations defined by dextran uptake, LYVE-1 expression, and MMP activity. (A–E) Flow cytometric analysis of single cells isolated from tumors from MMTV-PyMT/c-fms-EGFP mice treated for 2–7 wk with M279 or rat IgG and injected with 10 kDa dextran 1–2 h before tissue collection. (A) Characterization of dextran-positive myeloid cells using cell surface markers F4/80, CD11c, and Gr-1. (B) Representative plots showing the dextran-positive cells within the CD45$^+$ EGFP$^+$ F4/80$^+$ population in M279- and IgG-treated tumors. (C) Quantification of the frequency of tumor F4/80$^+$ and F4/80$^+$ dextran-positive cells using the gating strategy shown in B. Graph depicts means ± SD as percentages of total single cells, normalized to the mean percentage of F4/80$^+$ cells in IgG group, n = 7 mice (IgG) or 11 mice (M279) per group, ***P < 0.001. (D) Proportion of dextran-positive cells out of F4/80$^+$ cells in the tumor after M279 or IgG treatment. n = 7 mice (IgG) or 11 mice (M279) per group, n.s., not significant. (E) Representative histograms characterizing the phenotype of dextran-positive or -negative, EGFP$^+$ F4/80$^+$ cells in IgG- and M279-treated tumors. Note that all dextran-positive cells express CD11c, whereas the dextran-negative F4/80$^+$ population includes some CD11c$^-$ cells; the dextran-negative population also contains more F4/80 low cells (red arrows). (F) MMR (red) staining of tumor cryosections from mice treated with M279 or IgG from 8.5 wk (palpable stage) to 17 wk old. Note that most stromal myeloid cells are positive for MMR, unlike the more sparse myeloid cells within the tumor mass. (G) Tumor cryosections from mice treated with M279 or IgG for 7 wk starting at 4.5 wk of age. Cells that take up dextran (yellow arrows) are also marked by LYVE-1, and are depleted in M279-treated tumors. (H) Still frames from intravital imaging of an untreated MMTV-PyMT/c-fms-EGFP/ACTB-ECFP mouse injected with MMPSense 680 probe (pseudocolored red) 24 h before imaging, and rhodamine-labeled 10 kDa dextran (pseudocolored pink) 20 min after imaging started. Dextran in blood vessels (pink arrow) leaks out to the stroma. A large portion of myeloid cells display MMP activity (orange arrows), and take up dextran (white arrows). Colocalization of ingested dextran (green) and MMP activity (red) is shown in the close-up on the right. (I) Still frames from intravital time-lapse imaging of MMTV-PyMT/c-fms-EGFP/ACTB-ECFP mice treated with M279 or IgG for 3.5 wk, starting at 12 wk of age. MMPSense 680 probe (pseudocolored red) was injected intravenously 24 h before imaging, a fluorescently labeled Gr-1 antibody (pseudocolored green) 1 h before imaging, and fluorescent 10 kDa dextran (pseudocolored pink) a few minutes after imaging was started. White arrows point to MMPSense$^+$ cells that take up dextran; green arrows mark examples of Gr-1$^+$ cells. The close-up in the middle shows that Gr-1$^+$ neutrophils (green) do not display MMP activity (red). (Scale bars, 50 μm.)

contrast to tumors, these circulating cells were mostly CD11c$^-$, but nevertheless were almost completely eradicated by M279 treatment (Fig. 3 F and H). The depletion of this population, which has been suggested to replenish tissue resident macrophages selectively (21), provides one plausible explanation for the observed lack of recruitment of new M-DCs into M279-treated tumors.

In blood, a smaller proportion but wider variety of cells than in tumors took up injected dextran (Fig. S3C), but the dextran-positive population was still depleted by M279 treatment, especially the cells positive for both F4/80 and dextran (Fig. 3 G and H).

**Prolonged Anti–CSF-1R Treatment Delays Breast Tumor Growth.** The first tumors in MMTV-PyMT mice transition from adenoma/MIN stage to malignant early carcinoma at 8–9 wk of age, a process that coincides with sharply increased macrophage infiltration and activation of angiogenesis (12). TAM depletion alone can reduce tumor growth in some models but not others (8, 21, 39). We therefore tested whether the efficient depletion of M-DCs achieved by M279 treatment was therapeutic in the MMTV-PyMT model. We administered M279 or control rat IgG from 8.5 wk of age, when first palpable tumors were detected, to 17 wk when all mice had metastases to the lung (Fig. 4A). M279 treatment
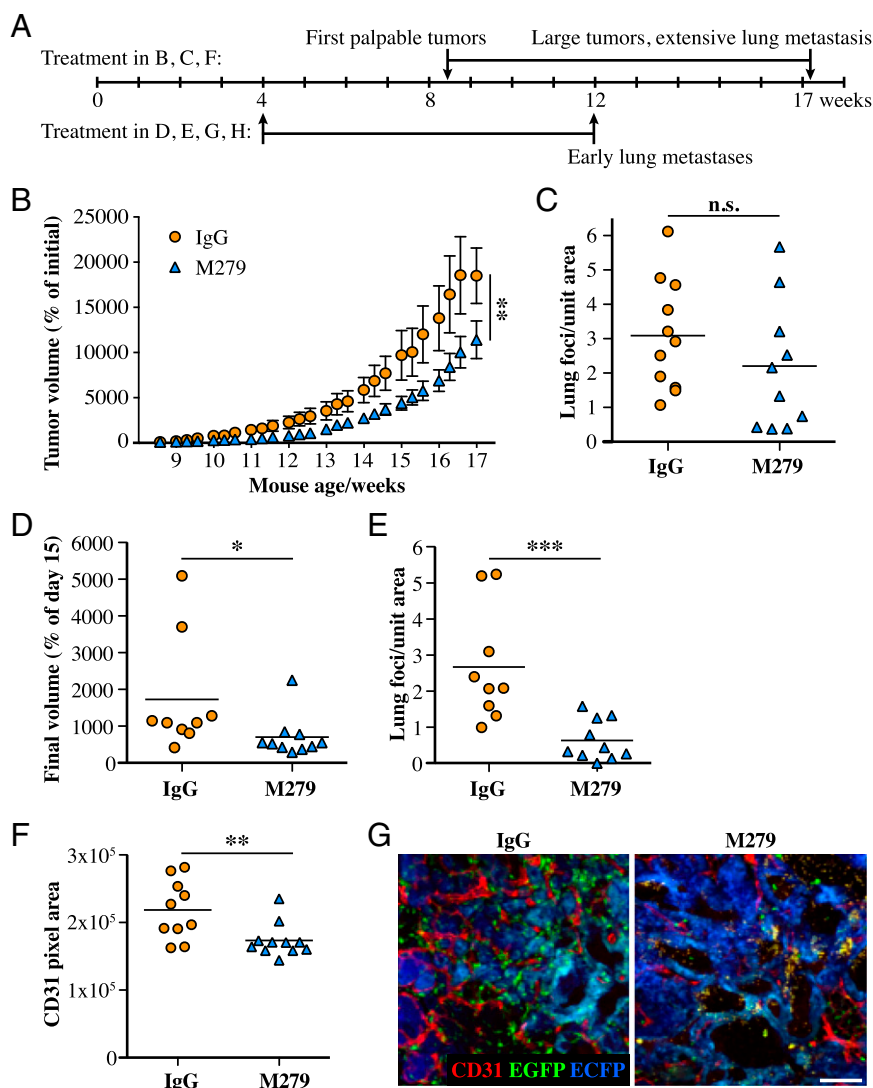
**Fig. 3.** Anti–CSF-1R antibody M279 causes myeloid cell death and blocks their recruitment to tumors. (*A*) Cryosections of tumor tissue from MMTV-PyMT/c-fms-EGFP mice treated with M279 or IgG for 2 wk, starting at 10 wk of age. Mice were injected intravenously with rhodamine-labeled 10 kDa dextran at the start of treatment to label preexisting myeloid cells (Dextran 1, red). AF647-labeled 10 kDa dextran (Dextran 2, pseudocolored green) was injected at the end point to mark cells that accumulated during treatment. Yellow arrows point to preexisting cells that have taken up both dextrans, whereas green arrows mark cells positive only for Dextran 2, newly accumulated during the treatment. (Scale bar, 50 μm.) (*B*) Quantification of the results shown in *A*. Graph depicts means + SD, $n = 3$ mice in IgG group, 6 mice in M279 group. (*C*) Still frames from intravital imaging of MMTV-PyMT/c-fms-EGFP mice treated with M279 or IgG for 4 d, starting at 16 wk of age. Red arrows point to examples of dying myeloid cells (green) labeled by propidium iodide (red) in the M279-treated tumor. (Scale bar, 100 μm.) (*D–H*) Flow cytometric analysis of peripheral blood from MMTV-PyMT/c-fms-EGFP mice treated for 3–7 wk with M279 or IgG. (*D*) Representative plots showing the frequency of CD45^{+} EGFP^{+} cells in peripheral blood. (*E*) Characterization of EGFP^{+} cells in the blood from IgG control mice. Note the lack of an obvious CD11c^{+} population. (*F*) Representative plots displaying Gr-1^{+} and F4/80^{+} cells within the CD45^{+} EGFP^{+} gate (*D*) in the blood of M279- or IgG-treated mice. (*G*) Representative plots evaluating dextran uptake in F4/80^{+} EGFP^{+} cells in the blood of M279- or IgG-treated mice. (*H*) Quantification of the frequency of myeloid cells in the blood from IgG- or M279-treated mice using gating strategies illustrated in *D*, *F*, and *G*. Graph depicts means ± SD as percentages of total single cells, $n = 7$ mice (IgG) or 8 mice (M279) per group, $**P < 0.01$, $***P < 0.001$.

**Fig. 4.** Anti-CSF-1R treatment attenuates tumor growth, early lung metastasis and tumor angiogenesis. (*A*) Schematic representation of treatment regimens used. (*B*) MMTV-PyMT/c-fms-EGFP mice bearing their first palpable tumors were treated with M279 or IgG for 60 d. Tumor volumes were normalized to the volume on treatment day 1, and the mean total tumor volumes ± SEM per treatment group are shown as a function of time. $n = 11$ mice per group. (*C*) Quantification of lung metastatic foci per unit area in paraffin sections from the experiment described in *B*. (*D*) Four-week-old MMTV-PyMT/c-fms-EGFP/ACTB-ECFP mice were treated with M279 or IgG for 56 d. End-point tumor volumes are plotted as percentages of volumes at day 15, when all mice had their first palpable tumors. $n = 9$ or 10 mice per group. (*E*) Quantification of lung metastatic foci per unit area in paraffin sections from the experiment described in *D*. (*F*) Quantification of pixel area positive for pan-endothelial marker CD31 in tumor cryosection micrographs from the experiment described in *D*. (*G*) Representative images from CD31-stained tumor cryosections from M279- and IgG-treated mice described in *D*. (Scale bar, 100 μm.) For all graphs, *$P < 0.05$, **$P < 0.01$, ***$P < 0.001$, n.s., not significant.

resulted in a modest but statistically significant ($P < 0.05$) delay in tumor growth as measured by total tumor burden (Fig. 4*B*), and a similar trend was observed when the experiment was repeated with smaller groups of mice (Fig. S4*A*). The treated tumors showed no obvious qualitative differences in tumor grade (Fig. S4*B*) or extent of tumor necrosis (Fig. S4*C*), indicating that a block in progression to advanced carcinoma was not the cause of reduced tumor growth. The average number of metastatic foci per lung area was lower in the M279-treated mice compared with control mice (Fig. 4*C*), although the mice in both treatment groups had extremely variable lung metastatic burdens.

**Early Anti–CSF-1R Treatment Inhibits Lung Metastasis and Tumor Angiogenesis.** To analyze the effects of myeloid cell depletion on the early events involved in transition to malignancy and initiation of metastasis, we applied a prolonged treatment protocol starting at the hyperplastic stage at 4 wk of age before the

beginning of extensive macrophage infiltration, initiation of angiogenesis, and invasion/metastasis, with the end point set at 12 wk, when the first macrometastases are seen in the lungs of MMTV-PyMT mice (Fig. 4*A*) (11, 40). Average myeloid cell depletion was over 85% (Fig. S4*D*). Importantly, in addition to delayed primary tumor growth (Fig. 4*D*), we now observed a significant decrease in the number of lung metastatic foci with M279 treatment (Fig. 4*E*), in agreement with observations that TAMs can support tumor cell intravasation in primary tumors and extravasation in metastatic lung (41, 42). Furthermore, we observed a small but significant decrease in area occupied by CD31+ endothelial cells in the MMTV-PyMT tumors treated with M279 from 4 to 12 wk (Fig. 4 *F* and *G*). This finding supports a link of macrophage depletion to decreased tumor angiogenesis, which is thought to be one of the major mechanisms by which antimacrophage therapies exert their effects (3, 8, 39).

**Lung Myeloid Cell Populations Are Minimally Affected by Anti–CSF-1R Treatment.** To determine if anti-CSF-1R treatment affects the myeloid compartment in the lung microenvironment, we analyzed metastatic lungs from MMTV-PyMT mice treated with M279 or IgG. The majority of myeloid cells in metastatic lungs were Gr-1$^+$ neutrophils and inflammatory monocytes (Fig. 5 *A–D*), as shown previously (43, 44). Surprisingly, we did not see an accumulation of macrophage- or DC-like cells, indicating that the overall composition of the immune infiltrate in the metastatic lung is distinct from the primary tumors (Fig. 5 *B–D*). As in the primary tumors and peripheral blood, the Gr-1 population did not change in response to M279 treatment (Fig. 5 *C* and *D*). In the lung, F4/80 expression was very low (Fig. 5*B* and Fig. S5*A*), and therefore we used CD11c as the marker for lung macrophages and DCs. In contrast to the primary tumor, the effect of antibody treatment on CD11c-expressing cells in the lungs was minimal. However, we did identify a small population of CD11c$^+$, c-fms-EGFP high cells, also expressing high levels of CD11b but low in F4/80 (Fig. 5*E*), which were depleted by M279 treatment (Fig. 5 *C–E*). Within this population, approximately half of the cells were dextran-positive (Fig. S5 *B* and *C*), and M279 treatment reduced their numbers (Fig. 5*E* and Fig. S5*C*). The minimal impact of the antibody on lung myeloid cells suggests that the antimetastatic efficacy of depleting CSF-1R–dependent cells early in tumor development results from its effects on the primary tumor.

## Discussion

In our study, we depleted CSF-1–dependent myeloid cells in a well-characterized, faithful model of human luminal-type breast cancer (45), and showed that this cell population conforms to both TAMs and TuDCs. We therefore chose to call them M-DCs. By real-time observation of stromal dynamics enabled by intravital microscopy (17) and by flow cytometric analysis, we discovered that the M-DC population contains subpopulations distinguished by endocytic ability, LYVE-1 expression, and MMP activity. These data show that, although published studies often refer to either TAMs or TuDCs, the F4/80-CD11c double-positive M-DCs in breast tumors actually share characteristics of both, and existing subgroups still conform to both phenotypes. Furthermore, our results elucidate the

mechanisms of CSF-1 function in tumors by showing that CSF-1R inhibition acted both by causing the death of established tumor-associated M-DCs and by blocking the accumulation of new M-DCs, possibly by depleting their supply from peripheral blood. Our study shows that M-DC depletion by sustained CSF-1R inhibition during multistage breast cancer progression delays tumor growth as monotherapy. However, the effect was relatively modest despite the prominence of the M-DC population in the primary tumors and the tumor trophic properties shown here and reported previously for TAMs. Treatment started in the initial stages of tumor development decreased tumor vascularization and blocked lung metastasis. CSF-1R blockage did not affect Gr-1–expressing neutrophils, which are important in supporting metastatic spread and tumor immune evasion (43, 44, 46). These results imply that although effective anti–CSF-1 strategies remove a very large myeloid population with multiple tumor trophic activities, combination treatments need to be used for effective therapeutic targeting of advanced breast cancer.

Although abrogation of CSF-1 signaling depletes myeloid cells defined as TAMs in several models (8, 10, 21, 39, 47–49), we found that the myeloid cell population depleted by M279 in MMTV-PyMT tumors matched the characterization of two phenotypes: TAMs and TuDC (20). This population expressed published markers of both macrophages and DCs, such as CSF-1R and F4/80 on the one hand, and CD11c and MHC II on the other. Dextran uptake has also been previously used to identify TAMs (24). However, TuDCs, which are a major antigen-presenting population in the tumors, engaging tumor-specific T cells in stable complexes and suggested to induce tolerance, also take up dextran (20). Accordingly, we called the myeloid population expressing both F4/80 and CD11c M-DCs. The presence of these antigen-presenting cells in tumors depended on CSF-1R signaling, as they were efficiently depleted by the M279 anti–CSF-1R antibody. The expression of LYVE-1, MMR, and MMP activity found in the dextran-positive subpopulation are characteristics previously identified with a M2-type polarization and trophic, angiogenic phenotypes (17, 27, 28, 30, 32). These properties have also been associated with Tie2-expressing monocytes, a strongly angiogenic, immunosuppressive myeloid subgroup in peripheral blood and tumors that are also present also in the MMTV-PyMT
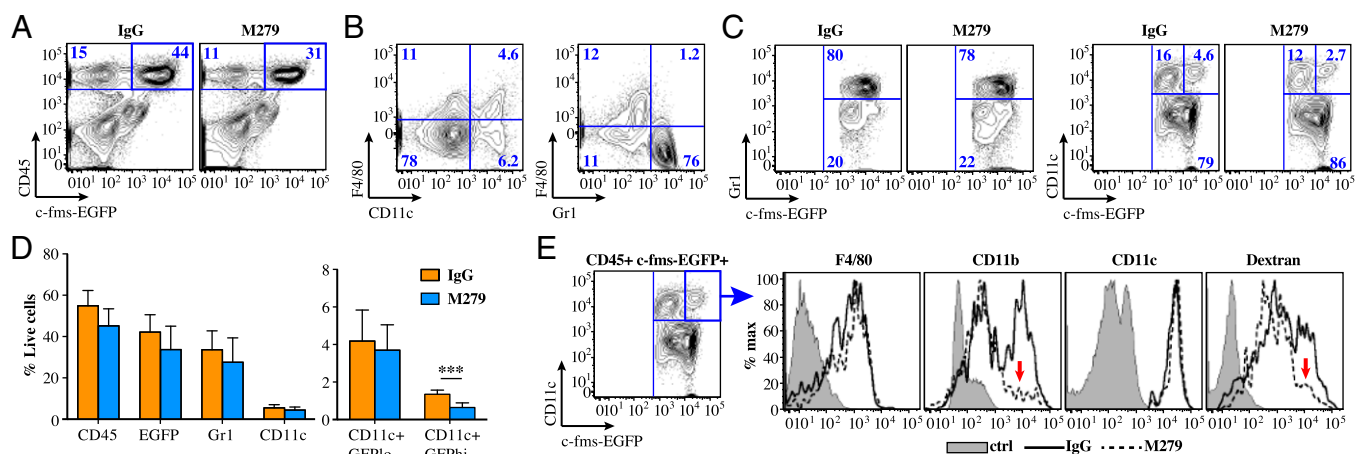


**Fig. 5.** Lung myeloid cells are minimally affected by CSF-1R blockade. Flow cytometric analysis of single cells isolated from metastatic lung tissue from MMTV-PyMT/c-fms-EGFP mice treated for 3–7 wk with M279 or IgG. (*A*) Representative plots showing the frequency of CD45$^+$ EGFP$^+$ single cells in lungs. (*B*) Characterization of myeloid cell subpopulations within the CD45$^+$ EGFP$^+$ gate in the IgG control of *A*. Note that less than 5% of EGFP$^+$ cells were CD11c$^+$ and F4/80$^+$, and the majority of myeloid cells in the metastatic lung are Gr-1$^+$ neutrophils/suppressor cells. (*C*) Analysis of Gr-1$^+$ and CD11c$^+$ cells within the CD45$^+$ EGFP$^+$ gate shown in *A*. An EGFP$^{hi}$, M279-sensitive subpopulation can be distinguished within the CD11c$^+$ myeloid population. (*D*) Quantification of the frequency of total immune cells (CD45$^+$) and subpopulations of myeloid cells in the lungs illustrated in *A* and *D*. Graph depicts means ± SD as percentages of total single cells, n = 5 mice (IgG) or 6 mice (M279) per group, ***$P < 0.001$. (*E*) Representative histograms characterizing the phenotype of CD11c$^+$ EGFP$^{hi}$ cells in IgG- and M279-treated metastatic lungs. The M279-sensitive population is characterized by high CD11b expression and ability to ingest dextran (red arrows).

Lohela et al.

model (28, 29, 50, 51). The CSF-1–dependent M-DC population clearly consists of further subpopulations, most likely including the Tie2-expressing monocytes. Interestingly, a recent study found that in the C57BL/6 background, the CD11b-F4/80 double-positive TAM population that becomes dominant as MMTV-PyMT tumors progress does not express the markers associated with M2 polarization, suggesting that there may be important strain-specific differences in tumor myeloid cell phenotypes (2).

We also found that a population of myeloid cells in peripheral blood with high expression of c-fms-EGFP and F4/80 was strongly depleted by prolonged M279 treatment. Moreover, we observed that very few new dextran-ingesting M-DCs accumulated in the tumor during M279 treatment. The depleted circulating cells are a subset of monocytes proposed to be committed to a resident tissue macrophage fate (21, 52). Our data are consistent with the hypothesis that CSF-1R signaling may be required for their maturation and acquisition of the "resident" phenotype, and possibly for survival in blood (21). Because this population is almost entirely absent after M279 treatment, it is still unclear whether anti–CSF-1R treatment also inhibits the actual migration/chemotaxis process of M-DC precursors into tumors. M-DCs present before the treatment were also depleted from tumors, and we directly observed dying myeloid cells during the first week of treatment, indicating that M-DCs depend on CSF-1 for survival in the tumor microenvironment. We cannot completely rule out that new M-DCs or their precursors were still recruited from blood during the 2-wk chase period, but could not survive in the tumor in the presence of M279. Furthermore, the M-DC population may expand by proliferating within the tumor, or a phenotypically distinct tumor-resident population of myeloid cells may differentiate to acquire the M-DC phenotype. Thus, the absence of new M-DCs in the tumor after M279 treatment could also be explained by blocked proliferation or differentiation.

Although we observed a delay in primary MMTV-PyMT tumor growth caused by prolonged treatment with the M279 anti–CSF-1R antibody as a single agent, some recent studies using small molecule inhibitors or antibodies to CSF-1 or CSF-1R did not (8, 21, 39). This difference most likely results from varying treatment schedules and relative specificity and potency of the inhibition. Furthermore, in CSF-1–null mutant mice, the majority of macrophages are absent, but the incidence and growth of MMTV-PyMT tumors is normal, although progression to metastatic late carcinoma is delayed (11). The roles of CSF-1 signaling during development are likely to be different from those in adult organisms and in tumor progression, and genetic background may also affect these results.

We found that blocking CSF-1R early during tumor progression reduced lung metastasis. Macrophage and monocyte populations have been reported to support the seeding of metastatic breast cancer cells in the lung, assisting their extravasation, secreting vascular endothelial growth factor and inducing angiogenesis, and they also promote the growth of metastatic lesions (12, 13, 41, 42, 53, 54). Macrophages support tumor cell migration and invasiveness by secreting chemotactic epithelial growth factor and matrix-remodeling proteases, such as cathepsins and MMPs (55–58). However, only a very minor lung myeloid cell population was affected by the M279 treatment. Thus, in our model the antimetastatic effect may have been mostly secondary to the depletion of trophic myeloid cells in the primary tumors. Our results, as well as a wide variety of other tumor models, show that myeloid cell depletion can abrogate tumor angiogenesis (14). Both macrophage infiltration and the subsequent onset of angiogenesis in the MMTV-PyMT model are closely associated with malignant transformation (12), and thus the early administration of M279 may have blocked the early stages of metastasis in the primary tumor rather than seeding and growth at the secondary sites.

Somewhat surprisingly, the observed efficient depletion of M-DCs, the largest infiltrating immune cell population in the MMTV-PyMT tumors, led to a relatively modest inhibition of tumor growth, metastasis, and angiogenesis. Our expectation was that TAMs would be trophic for tumors and that DCs would regulate tumor killing. However, because TuDCs do not support full activation or sustain cytolysis by cytotoxic T cells (20), their depletion may be of little consequence. This finding suggests that depletion of TAM function did not contribute substantially to tumor growth. These observations indicate that other cell types have important trophic functions in the MMTV-PyMT tumors and metastases. Significantly, CSF-1R targeting did not affect the Gr-1$^+$ neutrophil populations. Neutrophil-like myeloid-derived suppressor cells have been shown to have protumor functions, including growth factor secretion, angiogenic activity, and immunosuppression, and to be important in supporting metastatic spread (1, 4, 42–44, 46). In our study, intravital imaging demonstrated that the Gr-1$^+$ cells are highly motile and retained their capability to be recruited rapidly to sites of extensive cell death. However, although Gr-1$^+$ cells were abundant in metastatic lungs and peripheral blood, they were present in relatively small numbers in the primary tumors. It is likely that nonimmune cell types, such as carcinoma-associated fibroblasts, may be the key trophic stromal cells (1, 59).

The interplay between tumor cells and their stromal microenvironment continuously evolves during multistage cancer progression. The combination of intravital imaging of stromal dynamics in multistage tumor progression with specific, potent inhibition of a major myeloid cell signaling pathway has allowed us to deepen the understanding of the roles of different myeloid cell subgroups in breast cancer. CSF-1 signaling is required for M-DC accumulation and survival in the MMTV-PyMT model, and effective targeting of the CSF-1 pathway is therefore an attractive therapy prospect for human breast cancer and several other tumor types, given the association of macrophages and CSF-1 signaling with poor prognosis (3, 5–8). Indeed, another recently developed antibody against CSF-1R led to reductions in macrophages and clinical objective responses in a small cohort of patients with diffuse-type giant cell tumor, a rare proliferative disease driven by deregulated CSF-1 production; biopsies from patients with various solid tumor types also showed reduced macrophage numbers and somewhat increased CD8$^+$/CD4$^+$ T-cell ratios (10). However, in the MMTV-PyMT tumors, which closely model aggressive luminal B-type human breast cancer, the effects of M-DC depletion on tumor growth, angiogenesis, and metastasis remain insufficient to block progression. Small-molecule CSF-1R inhibitors that have had some success in inhibiting tumor growth in mouse models significantly affect other targets in addition to CSF-1R, and have mostly been used in combination with other therapy (5, 8, 39, 60). The results from our study also highlight the importance of acquiring a thorough understanding of the tumor trophic influences of various stromal players to effectively target the tumor microenvironment in cancer therapy. Combination therapy approaches that target several stromal components, as well as the tumor cells themselves, may be needed to overcome the complex microenvironmental machinery programmed to support tumor progression. Furthermore, our results indicate that efficient treatment of advanced breast cancer could benefit from combining targets that act more directly at the metastatic sites with antimacrophage strategies targeting the primary tumor. In our efforts to develop the right combinations for therapy, novel techniques, such as intravital imaging, can give us invaluable insight into how different interventions affect the growing, evolving tumor ecosystems.

## Materials and Methods

**Animals.** The MMTV-PyMT (40), ACTB-ECFP mice (61), and c-fms-EGFP (62) transgenic mouse lines were maintained in-house, all bred to at least sixth

generation FVB/N background, and crossed to double- or triple-transgenic mice for experiments. All animal experiments were conducted in accordance with protocols approved by the Institutional Animal Care and Use Committee at the University of California, San Francisco.

**Antibody Treatment of Mice.** Female MMTV-PyMT/c-fms-EGFP or MMTV-PyMT/c-fms-EGFP/ACTB-ECFP mice were treated with intraperitoneal injections of either rat M279 anti-CSF-1R antibody (provided by Amgen) (21) or rat IgG (Sigma-Aldrich), 400 μg per injection in 200 μL in PBS, three times per week for the times indicated. Tumor dimensions were measured with calipers at the time of each injection, and volumes were calculated using the formula width-squared times height multiplied by 0.52. Mice were perfusion-fixed with 1–2% paraformaldehyde (PFA) through the left ventricle, and tissue samples were collected and processed for (immuno)histological analysis and quantification (*SI Materials and Methods*). In other experiments, mice were injected intravenously with 100 μL of AF647-labeled 10 kDa dextran (4 mg/mL in PBS) (Life Technologies), and after 1–2 h perfused with 0.01 M EDTA in D-PBS to collect peripheral blood, and tissue samples were digested and processed to obtain single cell suspensions for FACS (*SI Materials and Methods*).

**Intravital Imaging.** The intravital spinning-disk confocal microscopy, surgical procedures, and anesthesia of mice were done as described previously (17), with some changes in equipment (*SI Materials and Methods*). Imaged mice were treated with M279 or IgG for the time stated in the figure and movie legends. Some mice were injected intravenously with 100–200 μL sterile PBS containing 4 mg/mL of 10 kDa, 70 kDa, or 2,000 kDa rhodamine-conjugated dextran and 4 mg/mL of 10 kDa AF488- or AF647-conjugated dextran (Life Technologies) just before or during imaging. Where indicated, propidium iodide (Life Technologies) was given intraperitoneally every hour, 66 μg/mL in 50 μL PBS. The MMPSense 680 reagent (PerkinElmer) was given intravenously in PBS 24–25 h before imaging, 2 nmol per mouse. Time-lapse videos were assembled using Bitplane Imaris (v6.3–7.6 for Windows 64×), adjusting brightness and contrast for clarity, as well as applying smoothing

filters to reduce noise. Datasets were corrected for respiratory motion artifacts using "drift correction" with spot detection of 10- to 20-μm diameter and Brownian motion algorithm with a maximum radius of 25–35 μm. Quantification of sessile dextran-positive cells in the movies was done by manually counting all positive cells from a time point 3–5 h after intravenous injection of 10 kDa or 70 kDa dextran, in four littermate pairs of mice treated with IgG or M279, and dividing the counts by the field of view area in each video. Over 50% depletion of myeloid cells was estimated by visual inspection, as were dead-cell–caused influx of myeloid cells, and presence or absence of myeloid cell death, defined as more than five propidium iodide-positive myeloid cells.

**Statistical Analyses.** The sum of the volumes of all tumors born by each mouse (total tumor volume) was calculated for every time point, and the mean total tumor volume for each treatment group was plotted as a function of time to obtain growth curves. The difference between groups was evaluated by repeated measures analysis of variance of transformed tumor volume data with Dunnett adjusted multiple comparisons (*SI Materials and Methods*), using JMP software v7.0 interfaced with SAS v9.1 (SAS Institute). For all other comparisons, Student $t$ tests were performed, using GraphPad Prism for Macintosh (v5.0d–6.0c; GraphPad Software). If necessary, variances were equalized with log transformation, or square-root transformation when a zero value measurement was present. For comparisons of more than two groups (FACS analysis), multiple comparisons were corrected for using the Holm–Sidak method.

1. Egeblad M, Nakasone ES, Werb Z (2010) Tumors as organs: Complex tissues that interface with the entire organism. *Dev Cell* 18(6):884–901.
2. Franklin RA, et al. (2014) The cellular and molecular origin of tumor-associated macrophages. *Science* 344(6186):921–925.
3. Qian BZ, Pollard JW (2010) Macrophage diversity enhances tumor progression and metastasis. *Cell* 141(1):39–51.
4. Gabrilovich DI, Ostrand-Rosenberg S, Bronte V (2012) Coordinated regulation of myeloid cells by tumours. *Nat Rev Immunol* 12(4):253–268.
5. Noy R, Pollard JW (2014) Tumor-associated macrophages: From mechanisms to therapy. *Immunity* 41(1):49–61.
6. Bingle L, Brown NJ, Lewis CE (2002) The role of tumour-associated macrophages in tumour progression: Implications for new anticancer therapies. *J Pathol* 196(3):254–265.
7. Leek RD, Harris AL (2002) Tumor-associated macrophages in breast cancer. *J Mammary Gland Biol Neoplasia* 7(2):177–189.
8. DeNardo DG, et al. (2011) Leukocyte complexity predicts breast cancer survival and functionally regulates response to chemotherapy. *Cancer Discov* 1(1):54–67.
9. Hume DA, MacDonald KP (2012) Therapeutic applications of macrophage colony-stimulating factor-1 (CSF-1) and antagonists of CSF-1 receptor (CSF-1R) signaling. *Blood* 119(8):1810–1820.
10. Ries CH, et al. (2014) Targeting tumor-associated macrophages with anti–CSF-1R antibody reveals a strategy for cancer therapy. *Cancer Cell* 25(6):846–859.
11. Lin EY, Nguyen AV, Russell RG, Pollard JW (2001) Colony-stimulating factor 1 promotes progression of mammary tumors to malignancy. *J Exp Med* 193(6):727–740.
12. Lin EY, et al. (2006) Macrophages regulate the angiogenic switch in a mouse model of breast cancer. *Cancer Res* 66(23):11238–11246.
13. Lin EY, et al. (2007) Vascular endothelial growth factor restores delayed tumor progression in tumors depleted of macrophages. *Mol Oncol* 1(3):288–302.
14. Coffelt SB, et al. (2010) Elusive identities and overlapping phenotypes of proangiogenic myeloid cells in tumors. *Am J Pathol* 176(4):1564–1576.
15. Hume DA (2011) Applications of myeloid-specific promoters in transgenic mice support in vivo imaging and functional genomics but do not support the concept of distinct macrophage and dendritic cell lineages or roles in immunity. *J Leukoc Biol* 89(4):525–538.
16. Geissmann F, Gordon S, Hume DA, Mowat AM, Randolph GJ (2010) Unravelling mononuclear phagocyte heterogeneity. *Nat Rev Immunol* 10(6):453–460.
17. Egeblad M, et al. (2008) Visualizing stromal cell dynamics in different tumor microenvironments by spinning disk confocal microscopy. *Dis Model Mech* 1(2-3):155–167, discussion 165.
18. Nakasone ES, et al. (2012) Imaging tumor-stroma interactions during chemotherapy reveals contributions of the microenvironment to resistance. *Cancer Cell* 21(4):488–503.
19. Mitchem JB, et al. (2013) Targeting tumor-infiltrating macrophages decreases tumor-initiating cells, relieves immunosuppression, and improves chemotherapeutic responses. *Cancer Res* 73(3):1128–1141.
20. Engelhardt JJ, et al. (2012) Marginating dendritic cells of the tumor microenvironment cross-present tumor antigens and stably engage tumor-specific T cells. *Cancer Cell* 21(3):402–417.
21. MacDonald KP, et al. (2010) An antibody against the colony-stimulating factor 1 receptor depletes the resident subset of monocytes and tissue- and tumor-associated macrophages but does not inhibit inflammation. *Blood* 116(19):3955–3963.
22. Bartocci A, et al. (1987) Macrophages specifically regulate the concentration of their own growth factor in the circulation. *Proc Natl Acad Sci USA* 84(17):6179–6183.
23. MacDonald KP, et al. (2005) The colony-stimulating factor 1 receptor is expressed on dendritic cells during differentiation and regulates their expansion. *J Immunol* 175(3):1399–1405.
24. Ojalvo LS, King W, Cox D, Pollard JW (2009) High-density gene expression analysis of tumor-associated macrophages from mouse mammary tumors. *Am J Pathol* 174(3):1048–1064.
25. Fleming TJ, Fleming ML, Malek TR (1993) Selective expression of Ly-6G on myeloid lineage cells in mouse bone marrow. RB6-8C5 mAb to granulocyte-differentiation antigen (Gr-1) detects members of the Ly-6 family. *J Immunol* 151(5):2399–2408.
26. Sasmono RT, et al. (2007) Mouse neutrophilic granulocytes express mRNA encoding the macrophage colony-stimulating factor receptor (CSF-1R) as well as many other macrophage-specific transcripts and can transdifferentiate into macrophages in vitro in response to CSF-1. *J Leukoc Biol* 82(1):111–123.
27. Mantovani A, Sozzani S, Locati M, Allavena P, Sica A (2002) Macrophage polarization: Tumor-associated macrophages as a paradigm for polarized M2 mononuclear phagocytes. *Trends Immunol* 23(11):549–555.
28. Pucci F, et al. (2009) A distinguishing gene signature shared by tumor-infiltrating Tie2-expressing monocytes, blood "resident" monocytes, and embryonic macrophages suggests common functions and developmental relationships. *Blood* 114(4):901–914.
29. De Palma M, et al. (2005) Tie2 identifies a hematopoietic lineage of proangiogenic monocytes required for tumor vessel formation and a mesenchymal population of pericyte progenitors. *Cancer Cell* 8(3):211–226.
30. Shaul ME, Bennett G, Strissel KJ, Greenberg AS, Obin MS (2010) Dynamic, M2-like remodeling phenotypes of CD11c+ adipose tissue macrophages during high-fat diet-induced obesity in mice. *Diabetes* 59(5):1171–1181.
31. Klimchenko O, et al. (2011) Monocytic cells derived from human embryonic stem cells and fetal liver share common differentiation pathways and homeostatic functions. *Blood* 117(11):3065–3075.
32. Cho CH, et al. (2007) Angiogenic role of LYVE-1–positive macrophages in adipose tissue. *Circ Res* 100(4):e47–e57.
33. Coussens LM, Tinkle CL, Hanahan D, Werb Z (2000) MMP-9 supplied by bone marrow-derived cells contributes to skin carcinogenesis. *Cell* 103(3):481–490.

34. Acuff HB, Carter KJ, Fingleton B, Gorden DL, Matrisian LM (2006) Matrix metalloproteinase-9 from bone marrow-derived cells contributes to survival but not growth of tumor cells in the lung microenvironment. *Cancer Res* 66(1):259–266.

35. Nozawa H, Chiu C, Hanahan D (2006) Infiltrating neutrophils mediate the initial angiogenic switch in a mouse model of multistage carcinogenesis. *Proc Natl Acad Sci USA* 103(33):12493–12498.

36. Erler JT, et al. (2009) Hypoxia-induced lysyl oxidase is a critical mediator of bone marrow cell recruitment to form the premetastatic niche. *Cancer Cell* 15(1):35–44.

37. Hiratsuka S, et al. (2002) MMP9 induction by vascular endothelial growth factor receptor-1 is involved in lung-specific metastasis. *Cancer Cell* 2(4):289–300.

38. Chitu V, Stanley ER (2006) Colony-stimulating factor-1 in immunity and inflammation. *Curr Opin Immunol* 18(1):39–48.

39. Priceman SJ, et al. (2010) Targeting distinct tumor-infiltrating myeloid cells by inhibiting CSF-1 receptor: Combating tumor evasion of antiangiogenic therapy. *Blood* 115(7):1461–1471.

40. Guy CT, Cardiff RD, Muller WJ (1992) Induction of mammary tumors by expression of polyomavirus middle T oncogene: A transgenic mouse model for metastatic disease. *Mol Cell Biol* 12(3):954–961.

41. Wyckoff JB, et al. (2007) Direct visualization of macrophage-assisted tumor cell intravasation in mammary tumors. *Cancer Res* 67(6):2649–2656.

42. Qian BZ, et al. (2011) CCL2 recruits inflammatory monocytes to facilitate breast-tumour metastasis. *Nature* 475(7355):222–225.

43. Yan HH, et al. (2010) Gr-1+CD11b+ myeloid cells tip the balance of immune protection to tumor promotion in the premetastatic lung. *Cancer Res* 70(15):6139–6149.

44. Kowanetz M, et al. (2010) Granulocyte-colony stimulating factor promotes lung metastasis through mobilization of Ly6G+Ly6C+ granulocytes. *Proc Natl Acad Sci USA* 107(50):21248–21255.

45. Lin EY, et al. (2003) Progression to malignancy in the polyoma middle T oncoprotein mouse breast cancer model provides a reliable model for human diseases. *Am J Pathol* 163(5):2113–2126.

46. Nagaraj S, Gabrilovich DI (2010) Myeloid-derived suppressor cells in human cancer. *Cancer J* 16(4):348–353.

47. Aharinejad S, et al. (2004) Colony-stimulating factor-1 blockade by antisense oligonucleotides and small interfering RNAs suppresses growth of human mammary tumor xenografts in mice. *Cancer Res* 64(15):5378–5384.

48. Aharinejad S, et al. (2002) Colony-stimulating factor-1 antisense treatment suppresses growth of human tumor xenografts in mice. *Cancer Res* 62(18):5317–5324.

49. Abraham D, et al. (2010) Stromal cell-derived CSF-1 blockade prolongs xenograft survival of CSF-1–negative neuroblastoma. *Int J Cancer* 126(6):1339–1352.

50. Coffelt SB, et al. (2010) Angiopoietin-2 regulates gene expression in TIE2-expressing monocytes and augments their inherent proangiogenic functions. *Cancer Res* 70(13):5270–5280.

51. Coffelt SB, et al. (2011) Angiopoietin 2 stimulates TIE2-expressing monocytes to suppress T cell activation and to promote regulatory T cell expansion. *J Immunol* 186(7):4183–4190.

52. Geissmann F, et al. (2010) Development of monocytes, macrophages, and dendritic cells. *Science* 327(5966):656–661.

53. Qian B, et al. (2009) A distinct macrophage population mediates metastatic breast cancer cell extravasation, establishment and growth. *PLoS ONE* 4(8):e6562.

54. Ferjančič Š, et al. (2013) VCAM-1 and VAP-1 recruit myeloid cells that promote pulmonary metastasis in mice. *Blood* 121(16):3289–3297.

55. Gocheva V, et al. (2010) IL-4 induces cathepsin protease activity in tumor-associated macrophages to promote cancer growth and invasion. *Genes Dev* 24(3):241–255.

56. Kessenbrock K, Plaks V, Werb Z (2010) Matrix metalloproteinases: Regulators of the tumor microenvironment. *Cell* 141(1):52–67.

57. Wyckoff J, et al. (2004) A paracrine loop between tumor cells and macrophages is required for tumor cell migration in mammary tumors. *Cancer Res* 64(19):7022–7029.

58. Condeelis J, Pollard JW (2006) Macrophages: Obligate partners for tumor cell migration, invasion, and metastasis. *Cell* 124(2):263–266.

59. Kraman M, et al. (2010) Suppression of antitumor immunity by stromal cells expressing fibroblast activation protein-alpha. *Science* 330(6005):827–830.

60. Pyonteck SM, et al. (2013) CSF-1R inhibition alters macrophage polarization and blocks glioma progression. *Nat Med* 19(10):1264–1272.

61. Hadjantonakis AK, Macmaster S, Nagy A (2002) Embryonic stem cells and mice expressing different GFP variants for multiple non-invasive reporter usage within a single animal. *BMC Biotechnol* 2:11.

62. Sasmono RT, et al. (2003) A macrophage colony-stimulating factor receptor-green fluorescent protein transgene is expressed throughout the mononuclear phagocyte system of the mouse. *Blood* 101(3):1155–1163.